Cell Proliferation

Cell Prolif., 2013, **46**, 685–694 doi: 10.1111/cpr.12072

Effects of TiO_2 nanotube layers on RAW 264.7 macrophage behaviour and bone morphogenetic protein-2 expression

S. J. Sun*,[1], W. Q. Yu*,[1], Y. L. Zhang*, X. Q. Jiang*,† and F. Q. Zhang*

**Department of Prosthodontics, Ninth People's Hospital, Shanghai Jiao Tong University School of Medicine, Shanghai Key Laboratory of Stomatology, Shanghai, 200011, China and* b*Oral Bioengineering Lab, Shanghai Research Institute of Stomatology, Ninth People's Hospital, Shanghai Jiao Tong University School of Medicine, Shanghai Key Laboratory of Stomatology, Shanghai, 200011, China*

Received 2 March 2013; revision accepted 21 July 2013

Abstract

Objectives: To investigate behaviour and osteogenic cytokine expression of RAW264.7 macrophages grown on TiO_2 nanotube layers.

Materials and methods: The murine macrophage cell line RAW 264.7 was cultured on TiO_2 nanotubes of varying diameter; macrophage morphology was examined using scanning electron microscopy. Cell adhesion and viability were assessed with the aid of the MTT method and *BMP-2* and *TGF-β* gene expression were examined by RT-PCR analysis. Levels of BMP-2, TGF-β1 and ICAM-1 proteins secreted into the supernatant were measured by ELISA assay.

Results: Macrophages cultured on nanotube layers had spread out morphology, the largest (120 nm) nanotube layer eliciting an elongation by 24 h. Macrophages adhered significantly less to 120 nm TiO_2 nanotubes than to control discs at 4 h after application; after 24 h incubation, macrophages were sufficiently viable ($P < 0.05$) on 30 and 70 nm nanotube layers. Increasing nanotube diameter led to increased BMP-2 protein secretion and increased BMP-2 mRNA expression.

Conclusion: These results demonstrate that nanoscale topography of TiO_2 nanotube layers can affect macrophage morphology, adhesion, viability and BMP-2 expression. Macrophages grown on layers of large nanotubes had the highest potential to enhance bone formation during bone healing.

[2]Correspondence: F. Q. Zhang, Department of Prosthodontics, Ninth People's Hospital, Shanghai Jiao Tong University School of Medicine, Shanghai 200011, China. Tel.: +86 21 23271699 (ext. 5694); Fax: +86 21 63136856; E-mail: fqzhang@vip.163.com

[1]Both authors contributed equally to this work.

Introduction

Titanium (Ti) and its alloys are often used as implant materials in orthopaedic and dental surgery as they have appropriate mechanical properties and are biocompatible with bone (1). Success of endosseous implants is related to achievement of osseointegration between surrounding bone and the implanted materials (2). Osseointegration can be enhanced by modifying properties of the implanted material's surface (such as topography and chemistry) (3). Recently, many reports have demonstrated that nanometer-scale surface features of Ti implants improve osteoblast adhesion and function *in vitro* and osseointegration *in vivo* (4–6).

Due to their potentially excellent bioactivity, ordered and controlled titanium oxide (TiO_2) nanotubes have received significant attention. Presence of TiO_2 nanotubes on the surface of Ti increases apatite formation (7). It has been demonstrated that TiO_2 nanotube layers provide a favourable template for bone cell (osteoblast or mesenchymal stem cell) growth and differentiation (5,8,9). When compared to bone cells grown on uncoated Ti or with Ti anodized nanoparticles, cells cultured on TiO_2 nanotube layers have higher adhesion, proliferation, alkaline phosphatase (ALP) activity and bone matrix deposition *in vitro* (9). Furthermore, it also has been demonstrated that presence of TiO_2 nanotube layers on Ti surfaces improves bone formation and enhances strongly adherent bone growth *in vivo* (6,10,11). Some reports indicate that adhesion, spreading, proliferation and differentiation of bone cells are critically dependent on tube dimensions (12–15). In a previous report from our laboratory, we showed that TiO_2 nanotubes measuring 20–70 nm effectively promoted MC3T3-E1 preosteoblast adhesion, and 70 nm TiO_2 nanotubes promoted cell ALP activity (1–3 weeks) and mineralization; additionally, we found that nanotubes measuring 100–120 nm did not bring forth these effects (12). Brammer *et al.* reported that 30 nm TiO_2

nanotubes promoted highest levels of MC3T3-E1 osteoblast adhesion, while those measuring 70–100 nm elicited a lower population of cells with elongated morphology and higher ALP activity (48 h) (13). According to work of Chamberlain *et al.*, 70 nm diameter nanotube surfaces had highest advantages in terms of diameter (30, 50 and 100 nm) by producing weakest inflammatory responses (16). These results all indicate that dimensions of TiO_2 nanotubes play an important role in developing cell behaviour.

Macrophages also play a critical role in determining biological responses at endosseous implant surfaces (17,18). In addition to osseointegration, initial stabilization of endosseous implants (which most likely depend on characteristics of early wound healing), is also important for successful restoration. Macrophages, including monocyte-derived macrophages and resident tissue macrophages, play an important part in wound healing (19). At the time of implantation, monocytes can migrate into fibrin blood clots of implants (20). Such monocytes rapidly acquire certain macrophage phenotypic traits and give rise to resident macrophages' on arrival at the wound. Macrophages contribute additional growth factors, chemokines and cytokines to modulate the healing process in the niche (17). Among these molecules, the transforming growth factor beta (TGF-β) family receives much attention as these factors are essential for repair. Lucas *et al.* confirmed reduction in TGF-β1 protein in macrophage-depleted animals and correlated this reduction with inability either to generate granulation tissue or to form a normal scar (19). Bone morphogenetic proteins (BMPs), which are members of the TGF-β superfamily, play a central role in induction of osteogenic cells from pluripotent mesenchymal stem cells (21), and BMP-2, -4, -6 and -7 are all expressed in wound tissues (22). It has been suggested that macrophages can adhere to endosseous implants and act as an important source of osteoinductive cytokines (23,24). Recently, Takebe and coworkers demonstrated that macrophages express BMP-2 mRNA and TGF-β1 mRNA (23). They also reported that properties of implants, such as their topography and chemistry, influence BMP-2 mRNA expression of macrophages *in vitro* (24). For implants with rough surfaces, enhanced macrophage accumulation is associated with more rapid bone-like tissue production (25). All these investigations suggest that macrophages play an essential role during osseous wound healing, at the implant surface, and might even contribute surface-dependent osteoinductive signals. At present, few studies of macrophages cultured on nanotube layers exist, and the macrophage osteoinductive phenotype, and its potential modulation by TiO_2 nanotube layers, has remained unknown.

Here, to investigate behaviour and osteogenic cytokine expression of RAW264.7 macrophages grown on TiO_2 nanotube layers, morphology, adhesion, proliferation and *BMP-2* and *TGF-β1* expression of RAW264.7 macrophages cultured on TiO_2 nanotubes with varying diameters, were evaluated *in vitro*.

Materials and methods

Sample preparation

Ti thin foils, 0.25 mm thick, 99.5% pure (Alfa Aesar, Ward Hill, MA, USA) were used to prepare the samples. Prior to anodization, Ti substrates were immersed in a mixture of 2 ml 48% HF, 3 ml 70% HNO_3 (both reagent grade chemicals) and 100 ml deionized water for 5 min, to remove the oxide layer that naturally forms on Ti materials. Next, substrates were rinsed in deionized water and dried under a nitrogen stream. TiO_2 nanotubes were fabricated by anodization with a potentiostat in 0.5 wt.% HF solution at 5, 15 and 25 V for 3 h; platinum was used as the counter electrode. After anodization, samples were rinsed in deionized water and dried under a nitrogen stream. To crystallize the as-deposited amorphous-structured TiO_2 nanotubes, nanotubes were then sintered at 500 °C for 2 h; then, nanotube layers were characterized as in our previously reported work (12,26). Diameters of nanotube layers were approximately 30, 70 and 120 nm under 5, 15 and 25 V, respectively (Fig. 1). Ti foils were polished using SiC emery paper (No. 1200 grit size) for use as control samples (denoted 'ctrl'). Prior to culture seeding, each experimental disc (1×1 cm^2) was sterilized in a steam autoclave at 120 °C for 30 min.

Cell culture

Mouse macrophage cell line RAW 264.7 (ATCC No. TIB 71) was obtained from the Chinese Academy of Science Cell Bank (Shanghai, China). Cells were cultured at 1.5×10^5 cells/cm^2 in Dulbecco's modified Eagle's medium supplemented with 10% foetal bovine serum (Gibco-BRL, Grand Island, NY, USA) and 1% penicillin / streptomycin, in a humidified incubator (37 °C; 5% CO_2); they were passaged every third day. The cells were then seeded on to discs in 24-well polystyrene culture plates (Falcon, Becton Dickinson, NJ, USA) at 1.5×10^5 cells/cm^2. For scanning electron microscopy (SEM), cells were seeded on to discs at 1.5×10^4 cells/cm^2.

Cell morphology

RAW264.7 cell morphology on each disc type was examined using SEM. Cells that had been incubated on

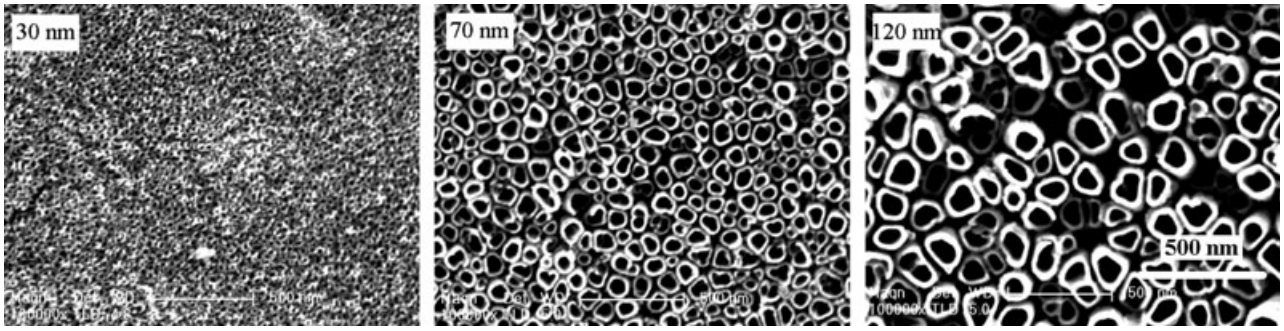

Figure 1. Scanning electron microscopy micrographs (top view) of TiO_2 nanotube layers with different diameters. The images show highly ordered nanotubes with 3 different nanotube diameters, including 30, 70 and 120 nm, fabricated by controlling anodizing potential in the range from 5, 15 and 25 V.

discs for 4 and 24 h were rinsed twice in phosphate-buffered saline (PBS) and soaked in 2.5% glutaradehyde in 0.1 M PBS for 1 h at 4 °C. After fixation, they were rinsed three times in PBS for 10 min each. Samples were dehydrated in a graded series of alcohols (35, 50, 75, 90 and 100%) for 10 min each and subsequently were dried by supercritical point CO_2. SEM imaging was conducted on a field emission scanning electron microscope after sample surfaces were sputter coated in gold. Four images of separate random regions (×500) were taken, per disc. Cell area and cell elongation were used to assess differences in cell morphology observed by SEM results for 4 and 24 h culture. Each cell of interest was outlined by a single examiner, and its area was calculated using Image-Pros Plus 6.0 (Media Cybernetics, Silver Spring, MD, USA). Cell elongation, as indicated by ratio of long axis to short axis, was also measured by the analysis software (13,27).

Cell viability

Cell viability was assessed using the tetrazolium salt MTT method. RAW 264.7 macrophages were seeded on to discs and incubated for 4, 24, 48 and 72 h. Discs were transferred to new 24-well plates at defined time points, and culture medium was changed to 0.5 mg/ml MTT (Sigma Aldrich, St. Louis, MO, USA), under normal culture conditions for 4 h. Subsequently, medium was removed, and 200 µl DMSO was added to each well. Plates were shaken for 10 min and solutions were transferred to 96-multiwell plates; absorbance of each solution was measured at 490 nm using a spectrophotometer (Elx 800; BioTek, Winooski, VT, USA).

Cell adhesion

Cells cultured on samples for 4 and 24 h were washed in PBS then stained using the Viability/Cytotoxicity Assay Kit for Animal Live & Dead Cells (Biotium Inc, Hayward, CA, USA). In this assay, calcein AM stains live cells green, while EthD-III stains dead cells red. After 30 min incubation at room temperature, cells were observed by fluorescence microscopy (BX-60; Olympus, Hamburg, Germany). Five fields of view were imaged at random, and cells on each image were counted using Image-Pro Plus software (ver. 5.0).

RNA extraction and real-time quantitative RT-PCR analysis

After 24 and 72 h, discs were transferred to new 24-well plates. Total cell RNA extraction was performed using TRIzol Plus RNA purification kit (Invitrogen, Carlsbad, CA, USA) according to the recommended protocol. Quantity and quality of RNA obtained were analysed on a NanoDrop 1000 spectrophotometer (Thermo Scientific, San Jose, CA, USA) according to the manufacturer's instructions. Extracted RNA was subsequently reverse-transcribed to cDNA using a PrimeScript™_RT reagent kit (Takara Bio, Shiga, Japan). Gene-specific primers for *BMP-2*, *TGF-β1* and calibrator reference gene, *β-actin* were synthesized commercially (Shengong, Co. Ltd. Shanghai, China); specific primer sets are outlined in Table 1. All RT-qPCR reactions were performed using a MyiQ Single-Color real-time PCR Detection System (Bio-Rad Laboratories, Richmond, CA, USA). For quantitative PCR, 10 µl SYBR Premix Ex Taq™, 0.4 µl each forward and reverse primer and 1 µl cDNA template were used in a final reaction volume of 20 µl. Cycling conditions included an initial denaturation step of 180 s at 95 °C followed by 40 cycles of 10 s at 95 °C, 30 s at 60 °C, 30 s at 72 °C. Data collection was enabled at 72 °C in each cycle, and C_T (threshold cycle) values were calculated using iQ5 software (Bio-Rad Laboratories). Level of expression was normalized to *β-actin*. The analysis

Table 1. Nucleotide sequences for real-time RT-PCR primers

Gene	Primer sequence (forward/reverse)	Product size (bp)	Annealing temperature (°C)
β-actin	5′-GTGACGTTGACATCCGTAAAGA-3′ 5′-GCCGGACTCATCGTACTCC-3′	245	60
BMP-2	5′-TCTTCCGGGAACAGATACAGG-3′ 5′-TCTCCTCTAAATGGGCCACTT-3′	249	60
TGF-β1	5′-GCTCCCCTATTTAAGAACACCCAC-3′ 5′-CTCCCAAGGAAAGGTAGGTGATAG-3′	168	60

was based on calculating relative expression level of these genes compared to expression of controls at 24 h.

BMP-2, TGF-β1 and ICAM-1 protein secretion in RAW264.7 cell culture supernatants

BMP-2, TGF-β1 and ICAM-1 in the supernatant were evaluated using BMP-2, TGF-β1 and ICAM-1 Quantikine Enzyme-linked Immunosorbent Assay (ELISA) kits (R&D Systems, Minneapolis, MN, USA). Assays were performed precisely according to the manufacturer's instructions. After cells had been cultured on discs for 24 and 72 h (for measurements of ICAM-1, cells were cultured on disks for 4 and 24 h), culture supernatants were collected and centrifuged to remove particles, if any, and were then stored at −80 °C until use. For measurements of TGF-β1, ELISA was also performed as described previously (28). Cells were cultured in regular growth medium and allowed to attach for 4 h. Then, regular growth medium was replaced with serum-free medium 24 h before defined time points. Additionally, latent TGF-β1 was activated to immunoreactive TGF-β1 by acidification with 1 N HCl, for 10 min at room temperature. Samples were neutralized with 1.2 N NaOH/0.5 M 4-(2-hydroxyethyl)-1-piperazine ethanesulphonic acid (HEPES).

Statistical analysis

Data are expressed as mean ± standard deviation (SD). Statistical analysis was performed using one-way analysis of variance followed by Bonferroni multiple comparison to determine significance. Every experiment was repeated at least three times with separate cell preparations. Statistical analysis was performed using SPSS 11.0 software (SPSS, Chicago, IL, USA). Values of $P < 0.05$ were considered statistically significant.

Results

Cell morphology

Cell morphology on different diameter TiO_2 nanotube layers was examined using SEM. The images show that shapes of macrophages grown on control discs, and on the TiO_2 nanotube discs, were significantly different at every time point. At 4 h, RAW264.7 macrophages cultured on TiO_2 nanotube discs had elongated morphology, whereas those grown on control discs were nearly spherical with numerous microvilli or small protrusions visible on their surfaces (Fig. 2). Most cells adhered to nanotube layers had elongated bodies with numerous microvilli holding fast to the discs. These cell shape changes were reflected in larger elongation values observed for nanotube groups compared to control (ctrl) groups, as seen in the morphometric analysis (Table 2). This also shows that control groups had higher cell area value than nanotube groups, although the only significant difference recorded was between the control group and the 120 nm nanotube group.

After 24 h of culture, macrophages grown on nanotube discs had spread morphologies, with the largest diameter (120 nm) nanotube layer of elongated morphology (Fig. 2). Cells on control discs were rimmed by thin lamellae, or else were typically observed to be spherical and apparently stationary with no cell protrusions. Most cells on 30 and 70 nm nanotube layers were flat and extensively adherent to disc surfaces, while cells adhered to the 120 nm nanotube layer had elongated bodies and were characterized by unidirectional lamellipodial extensions. The control group had significantly lower cell area value than nanotube groups. In comparison, elongation value reached a maximum of 1.76705 for cells on 120 nm nanotube layers.

Cell viability

Results shown in Fig. 3 reveal that cell viability was affected by TiO_2 nanotube layers. In comparison to control discs, cell population numbers of TiO_2 nanotube groups fell with increasing nanotube diameter. However, the only significant difference observed in cell populations was identified between the control group and 120 nm group. With longer culture time, higher cell populations were observed for TiO_2 nanotube groups, specially for small nanotubes (diameter <100 nm). Cell populations of 30 and 70 nm nanotube groups were

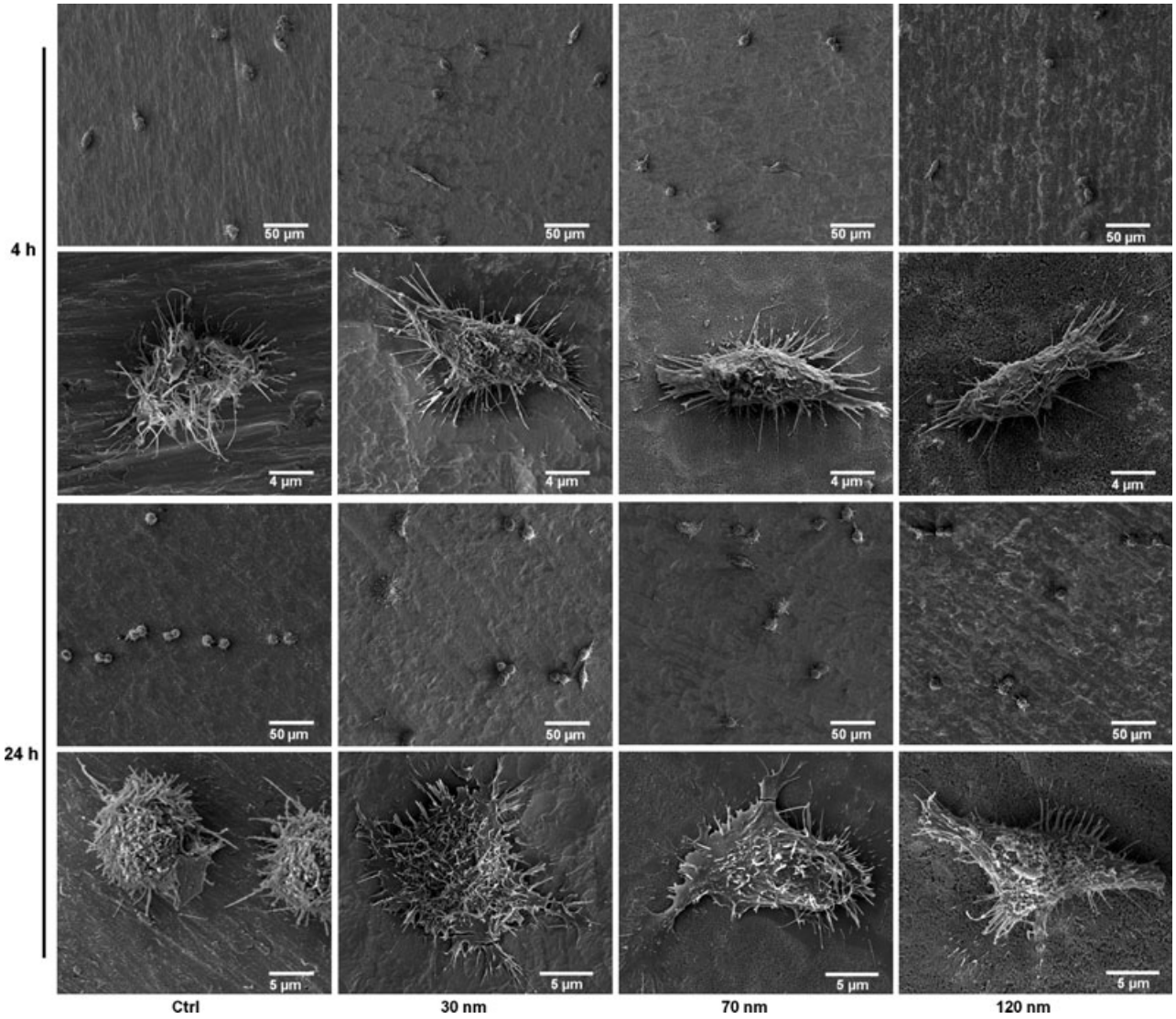

Figure 2. Low- and high-magnification scanning electron microscopy images of adherent RAW264.7 macrophages on control (ctrl), 30, 70 and 120 nm nanotube discs after 4 and 24 h. At 4 h, most cells adherent to nanotube layers displayed elongated bodies with numerous microvilli binding to the discs. At 24 h, cells on the 30 and 70 nm nanotube layers were flat and extensively adherent to disc surfaces, while cells adherent to 120 nm nanotube layers displayed elongated bodies and were characterized by unidirectional lamellipodial extensions. The control group had a significantly lower cell area value than the nanotube groups.

statistically higher than control groups after 48 h ($P < 0.05$). However, after 72 h, there was no significant difference in cell population sizes between groups.

Cell adhesion

As shown in Fig. 4, compared to control discs, cells adhered to 120 nm group TiO_2 nanotube layers were less than those of control groups at the earlier time point of 4 h ($P < 0.05$). However, after 24 h, cells on 30 and 70 nm nanotube layers were statistically higher than the control and 120 nm groups ($P < 0.05$).

BMP-2 and TGF-β1 mRNA levels in RAW264.7 macrophages

BMP-2 and TGF-β1 mRNA levels of macrophages grown on different discs are shown in Fig. 5. TiO_2 nanotube layer types significantly affected BMP-2 mRNA of adherent RAW264.7 macrophages (Fig. 5a). No difference was observed in BMP-2 mRNA expression among the four groups after 24 h; however, after 72 h, BMP-2 mRNA levels of TiO_2 nanotube groups were significantly higher than those of control groups ($P < 0.05$). Additionally, BMP-2 mRNA level increased with increase in

Table 2. Cell area and elongation measurements

	Ctrl	30 nm	70 nm	120 nm
Area (μm^2)				
4 h	185.568 ± 32.2782	171.755 ± 42.1980	162.808 ± 46.4406	155.955 ± 36.2662
24 h	142.105 ± 27.7634	234.687 ± 41.2608	211.504 ± 58.9566	203.228 ± 44.6075
Elongation				
4 h	1.43075 ± 0.248421	1.80067 ± 0.459767	1.73153 ± 0.475554	1.73079 ± 0.396955
24 h	1.18346 ± 0.125374	1.29039 ± 0.153369	1.41141 ± 0.224672	1.76705 ± 0.342328

Analysis of cell parameters (area and elongation) of RAW264.7 macrophages grown on control, 30, 70 and 120 nm nanotube discs after 4 and 24 h. Data presented as the mean ± SD ($n \geq 30$). Statistically significant differences are indicated (*significant at $P < 0.05$).

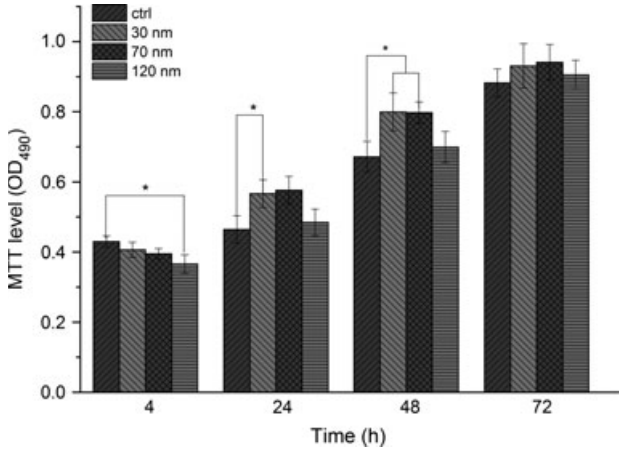

Figure 3. Cell populations on each disc type were assessed by MTT. Macrophages were seeded on discs for 4, 24, 48 and 72 h. Cell populations of the 30 and 70 nm nanotube groups were statistically greater than the control group after 48 h. After 72 h, there was no significant difference in cell population among all groups. Values are presented as the mean ± SD, $n = 3$. Statistically significant differences are indicated (*for $P < 0.05$).

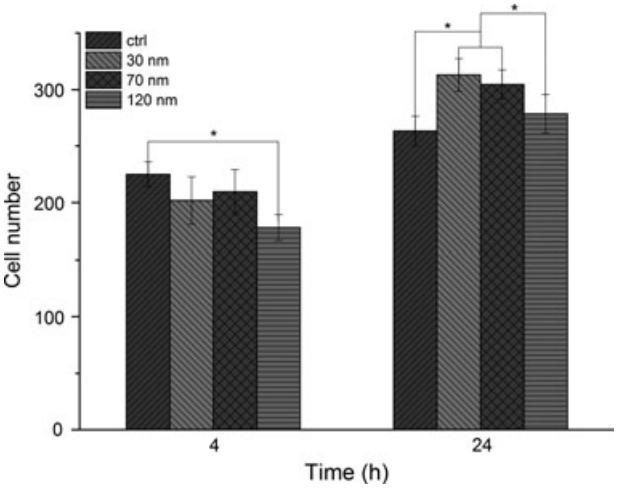

Figure 4. Cell counting of live/dead staining for MC3T3-E1 cells on control, 30, 70 and 120 nm nanotube discs after 4 and 24 h. Cells adherent to the 120 nm group TiO_2 nanotube layers were lower than those of the control groups at the earlier time point of 4 h. After 24 h, cells on 30 and 70 nm nanotube layers were statistically higher than the control and 120 nm groups. Values are presented as the mean ± SD, $n = 5$. Statistically significant differences are indicated (*for $P < 0.05$).

nanotube diameter. In contrast to BMP-2, TGF-β1 mRNA levels did not show significant effects related to surface topography at either 24 or 72 h (Fig. 5b). TGF-β1 mRNA level of control groups was higher than TiO_2 nanotube groups after 24 h in culture. However, at 72 h, the only significant difference was found between 30 and 120 nm nanotube groups ($P < 0.05$).

BMP-2, TGF-β1 and ICAM-1 secretion from RAW264.7 macrophages

BMP-2, TGF-β1 and ICAM-1 secretions from RAW264.7 cells grown on different discs are shown in Fig. 6. After 24 h culture, BMP-2 secretions of TiO_2 nanotube groups were higher than those of control groups, but there were no statistical differences ($P > 0.05$). By 72 h, BMP-2 secretions increased with increase in nanotube diameter. When cells were grown on 120 nm nanotube discs, BMP-2 secretion level was significantly higher (376.17 ± 47.26 pg/ml) than that of the other groups ($P < 0.05$), but for the first 24 h, TGF-β1 in the supernatant was almost indetectable. After 72 h culture, TGF-β1 secretion of controls was significantly

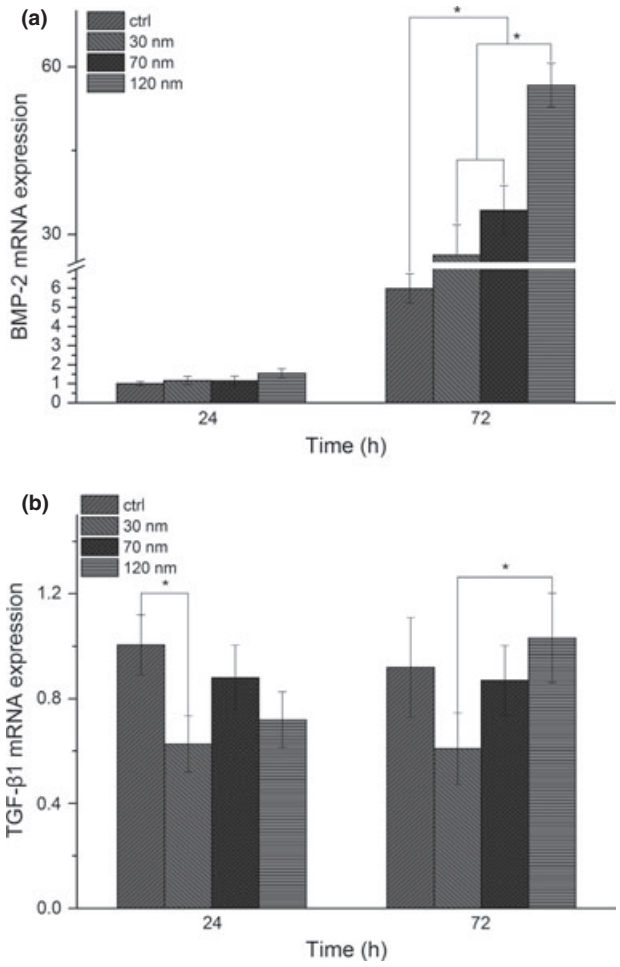

Figure 5. Evaluation of the BMP-2 and TGF-β1 mRNA levels in macrophages grown on control, 30, 70 and 120 nm nanotube discs for 24 and 72 h. (a) BMP-2 mRNA expression; (b) TGF-β1 mRNA expression. After 72 h, the BMP-2 mRNA levels of TiO_2 nanotube groups were significantly higher than the control group. TGF-β1 mRNA level, at 72 h, only significant difference was found between 30 and 120 nm nanotube group. Data are presented as the mean ± SD ($n = 3$). Statistically significant differences are indicated (*for $P < 0.05$).

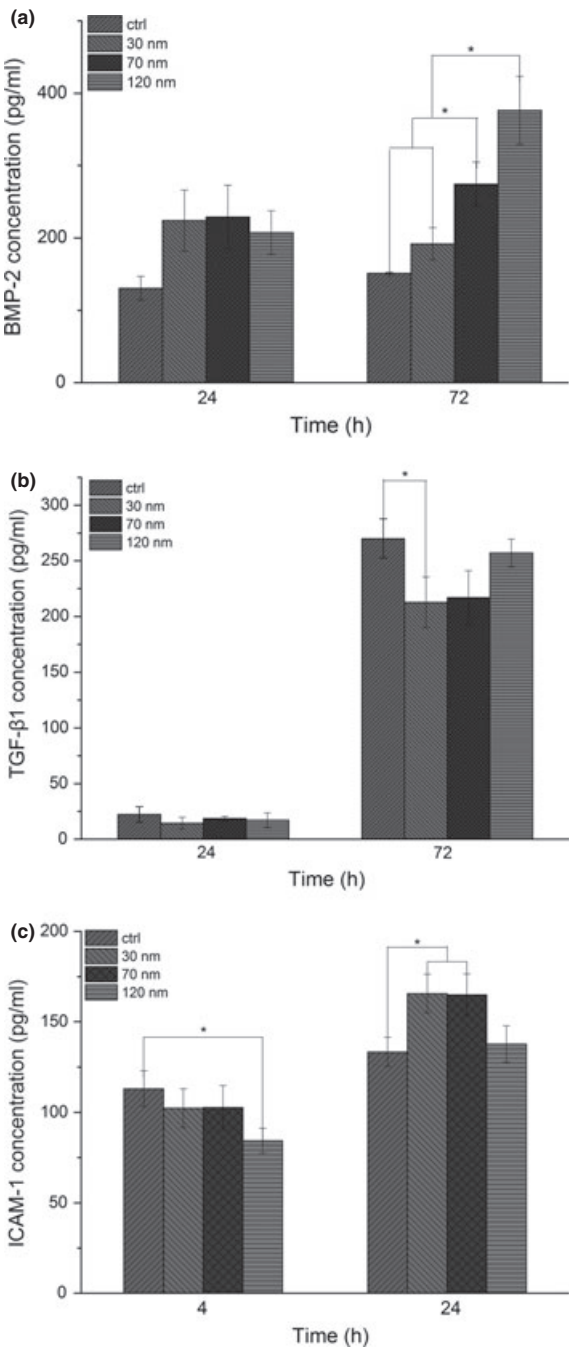

Figure 6. BMP-2 and TGF-β1 secretions from RAW264.7 cells grown on control, 30, 70 and 120 nm nanotube discs for 24 and 72 h. (a) Concentration of BMP-2; (b) Concentration of TGF-β1; (c) Concentration of ICAM-1. At 72 h, BMP-2 secretions increased with nanotube diameter. When cells were grown on 120 nm nanotube discs, BMP-2 secretion level was significantly higher than that of the other groups. After 72 h in culture, TGF-β1 secretion of the control was significantly higher than that of 30 nm nanotube groups. With respect to ICAM-1, after 24 h, the 30 and 70 nm nanotube groups were significantly higher than the control group. Data are presented as the mean ± SD ($n = 3$). Statistically significant differences are indicated (*for $P < 0.05$).

higher than that of 30 nm nanotube groups ($P < 0.05$). With respect to ICAM-1, at 4 h, only cells on 120 nm nanotube discs were lower than control groups ($P < 0.05$). After 24 h, 30 and 70 nm nanotube groups were significantly higher than control groups ($P < 0.05$).

Discussion

Macrophages play an essential role during osseous wound healing and might contribute surface-dependent osteoinductive signals. Hence, this work was carried out to investigate behaviour and osteogenic cytokine expression of RAW264.7 macrophages grown on TiO_2

nanotube layers. Results here show that macrophage morphology, adhesion, viability and BMP-2 expression were affected by topography of the TiO_2 nanotube layers. Those grown on large-diameter nanotube layers had the greatest potential to enhance bone formation during initial stages of bone healing.

Macrophage morphology on endosseous implant surfaces is affected by surface topography (24,29,30). In the present study, changes in shape of macrophages grown on nanotubes were found to be similar to changes exhibited by osteoblasts in similar conditions (13,15). Brammer *et al.* have found that large and thorough distribution of protein nanoparticles easily cover whole surfaces of 30 nm nanotubes, while proteins on 100 nm TiO_2 nanotubes only adhere sparsely at the top wall surface, due to presence of large empty nanotube pore spaces (13). Cells adherent to large nanotube layers have to expand their filopodia to find a protein-deposited surface, in the process forming exceedingly elongated shapes. Hence, after 24 h, macrophages adherent to large TiO_2 nanotube layers displayed elongated bodies. It was also found that cells adherent to small-diameter TiO_2 nanotube layers (30 and 70 nm) were flat and extensively bound to discs. This spreading morphology might be related to different formations of focal adhesions. Using atomic force microscopy and X-ray spectrometry (31), our previous study reported that nanoscale roughness of anatase type nanotube layers increased with increasing tube diameter, which usually means a larger surface area; however, adhesion of cells cultured on nanotube layers was inconsistent with nanomaterial characteristics. Moreover, it has been reported elsewhere that more protein tends to be deposited on surfaces of smaller diameter Ti nanotube layers, which may be a further reason that more cells adhered to these nanotubes, in our study (31).

Our investigation has demonstrated the ability of 120 nm TiO_2 nanotubes to discourage macrophage adhesion after 4 h culture. Previous studies have reported the influence of surface roughness on macrophage adhesion (32–34). Kim *et al.* reported that due to high degrees of nanometer-scale surface roughness, carbon nanotubes increase osteoblast and reduce macrophage adhesion (35). Khang *et al.* found that macrophage adhesion on conventional alumina (40 nm surface roughness) was significantly greater than on submicron alumina (50 nm surface roughness) and nanophase alumina (80 nm surface roughness) after 4 h (32). The summation of these results demonstrates that macrophage adhesion decreases with increasing surface roughness. Our group found that control discs exhibited lowest surface nanoroughness in comparison to the others, and that surface nanoroughness increased with diameter of the nanotube layers (12). Hence, differences in nanoroughness may cause reduction in macrophage adhesion to nanotubes with large diameters. In the present study, cells adherent to nanotubes of small diameter (30 and 70 nm) had significantly higher viabilities than those grown on control discs and large-diameter nanotubes after 24 and 48 h. Data presented here, using macrophages, are consistent with reports showing similar viability to osteoblasts and mesenchymal stem cells (12,14). Park *et al.* have reported that cells cultured on 100 nm TiO_2 nanotubes finally underwent anoikis, the adhesion-dependent form of cell death. They also reported that cells grown on 30 nm and smaller diameter TiO_2 nanotubes showed extensive formation of focal adhesions, while cells grown on 100 nm nanotubes formed only few focal adhesions (14). As macrophages are adhesion-dependent cells, those grown on large-diameter nanotubes may be driven to undergo cell death due to lack of focal adhesions. Gongadze *et al.* studied mechanisms of osteoblast adhesion to TiO_2 nanotubes and nanorough Ti surfaces, using a dynamic model (36,37). They found that strong attraction exists between cell membranes and small-diameter nanotube surfaces. They suggested that, compared to large-diameter nanotube surfaces, small-diameter nanotube surfaces on average have more sharp edges per unit area, with higher surface charge density, allowing integrin molecules to bind easily to neighbouring nanotubes on small-diameter nanotube surfaces. With respect to larger-diameter nanotube surfaces, integrin binding is more difficult, as these nanotubes have larger hollow interior spaces. This phenomenon could contribute to increased cell adhesion strength to lower diameter nanotube surfaces.

In addition to macrophage behaviour, expressions of BMP-2 and TGF-β1 in the macrophages adherent to varying diameter TiO_2 nanotube layers, were also evaluated. It has been reported that macrophage cytokine secretion can be affected by surface topography alone (micron- to submicron-scale), without modification of surface chemistry (24,29). Cooper and colleagues investigated osteogenic cytokine expression of macrophages grown on submicron-scale topography surfaces of Ti. These discs have different surface roughness characteristics, for example discs polished to 600-grit roughness (0.6 μm surface roughness) and discs finished by grit-blasting with 50-μm Al_2O_3 particles (1.2 μm surface roughness) (24). These authors confirmed that submicron-scale surface topography of Ti implants modulated BMP-2 expression in macrophages (24,30). Experts also have reported that surface topography can modulate activation of the NFκB pathway in macrophages through lipid rafts (34). In the present study, discs with nanotube layers measuring 30, 70 and 120 nm were used. Based on our previous study, surface roughness of these

nanotube layers can be expressed in nanometers, and surface nanoroughness of substrates increased with dimensions of TiO_2 nanotube layers (12). Our group originally found that nanoscale surface topography can influence BMP-2 expression in macrophages. After 72 h, expression of BMP-2 mRNA and secretion of BMP-2 in macrophages grown on TiO_2 nanotubes, increased proportionally with increasing size of TiO_2 nanotube pores. Promotion of this expression might be related to surface topography or roughness (34,38); however, more experiments must be performed to identify the mechanisms involved. In contrast to BMP-2, TGF-β1 expression was not significantly affected by surface topography. This result is consistent with studies of Takebe *et al.* (24). Surface microtopography has been suggested to positively influence blood clot formation, blood clot retention and bone formation, in peri-implant bone healing (30,39). It has been confirmed that TiO_2 nanotube implants increase osseointegration strengths, new bone formation and bone-implant contact after 4–6 weeks, in rabbit tibia (10,11).

According to our results, larger-diameter nanotube surfaces had effects on both enhancing and adhesion reduction. Marchisio *et al.* performed an analysis on response of RAW 246.7 cells to different Ti surfaces and found that cells cultured on rougher surfaces had higher ability to differentiate, in addition to lower adhesion ability (40). These authors believed that surfaces with more peaks and valleys could account for organization of cell clusters, which in turn, might explain high levels of differentiation observed on such surfaces. However, a smoother surface can enhance cell orientation and adhesion. Kim *et al.* studied TNF-α and LPS-activated RAW 264.7 cells. They found that AMPK inhibitor compound C, could inhibit ICAM-1 and VCAM-1 expression in addition to inhibiting phosphorylation of PI3K and p38 MAP kinase (41). This may be one of the mechanisms of bone formation enhancing and adhesion reducing effects of large-diameter nanotube surfaces. TiO_2 nanotube layers on implant surfaces may not only affect osteoblasts but also might influence macrophages with respect to enhancing bone formation in peri-implant bone healing.

In conclusion, here we have demonstrated that macrophage morphology, adhesion, viability and BMP-2 expression were affected by TiO_2 nanotube layers. After 24 h incubation, RAW 264.7 macrophages presented sufficient adhesion and viability on 30 and 70 nm nanotube layers, but not on 120 nm nanotube layer. Macrophages cultured on nanotube discs had spread out morphology, while 120 nm nanotube layers were elongated in shape. A trend was revealed in which increasing nanotube diameters led to increased BMP-2 protein secretion, together with increased BMP-2 mRNA expression. Based on all these results, macrophages grown on large-diameter nanotube layers had the greatest potential to enhance bone formation during initial stages of bone healing.

Acknowledgements

This work was supported by grants from the Shanghai Leading Academic Discipline Project (No. S30206, T0202), the Science and Technology Committee of Shanghai (No. 08DZ2271100, 1052 nm 04300 and 10JC1408600) and National Natural Science Foundation of China (81070866). The authors thank Xiuli Zhang (Oral Bioengineering Lab, Ninth People's Hospital, Shanghai Jiao Tong University School of Medicine) for her helpful assistance with the experiments.

References

1 Albrektsson T, Wennerberg A (2004) Oral implant surfaces: part 2 – review focusing on clinical knowledge of different surfaces. *Int. J. Prosthodont.* **17**, 544–564.
2 Buser D, Nydegger T, Oxland T, Cochran DL, Schenk RK, Hirt HP *et al.* (1999) Interface shear strength of titanium implants with a sandblasted and acid-etched surface: a biomechanical study in the maxilla of miniature pigs. *J. Biomed. Mater. Res.* **45**, 75–83.
3 Albrektsson T, Wennerberg A (2004) Oral implant surfaces: part 1 – review focusing on topographic and chemical properties of different surfaces and in vivo responses to them. *Int. J. Prosthodont.* **17**, 536–543.
4 Sato M, Aslani A, Sambito MA, Kalkhoran NM, Slamovich EB, Webster TJ (2008) Nanocrystalline hydroxyapatite/titania coatings on titanium improves osteoblast adhesion. *J. Biomed. Mater. Res. A* **84**, 265–272.
5 Kim JH, Cho KP, Chung YS, Kim OS, Chung SS, Lee KK *et al.* (2010) The effect of nanotubular titanium surfaces on osteoblast differentiation. *J. Nanosci. Nanotechnol.* **10**, 3581–3585.
6 Von Wilmowsky C, Bauer S, Lutz R, Meisel M, Neukam FW, Toyoshima T *et al.* (2009) In vivo evaluation of anodic TiO_2 nanotubes: an experimental study in the pig. *J. Biomed. Mater. Res. B Appl. Biomater.* **89B**, 165–171.
7 Tsuchiya H, Macak JM, Müller L, Kunze J, Müller F, Greil P *et al.* (2006) Hydroxyapatite growth on anodic TiO_2 nanotubes. *J. Biomed. Mater. Res. A* **77A**, 534–541.
8 Yao C, Slamovich EB, Webster TJ (2008) Enhanced osteoblast functions on anodized titanium with nanotube-like structures. *J. Biomed. Mater. Res. A* **85**, 157–166.
9 Popat KC, Leoni L, Grimes CA, Desai TA (2007) Influence of engineered titania nanotubular surfaces on bone cells. *Biomaterials* **28**, 3188–3197.
10 Bjursten LM, Rasmusson L, Oh S, Smith GC, Brammer KS, Jin S (2010) Titanium dioxide nanotubes enhance bone bonding in vivo. *J. Biomed. Mater. Res. A* **92**, 1218–1224.
11 Sul YT (2010) Electrochemical growth behavior, surface properties, and enhanced in vivo bone response of TiO_2 nanotubes on microstructured surfaces of blasted, screw-shaped titanium implants. *Int. J. Nanomed.* **5**, 87–100.
12 Yu WQ, Jiang XQ, Zhang FQ, Xu L (2010). The effect of anatase TiO_2 nanotube layers on MC3T3-E1 preosteoblast adhesion,

proliferation, and differentiation. *J. Biomed. Mater. Res. A* **94**, 1012–1022.
13 Brammer KS, Oh S, Cobb CJ, Bjursten LM, van der Heyde H, Jin S (2009) Improved bone-forming functionality on diameter-controlled TiO_2 nanotube surface. *Acta Biomater.* **5**, 3215–3223.
14 Park J, Bauer S, von der Mark K, Schmuki P (2007) Nanosize and vitality: TiO_2 nanotube diameter directs cell fate. *Nano Lett.* **7**, 1686–1691.
15 Oh S, Brammer KS, Li YS, Teng D, Engler AJ, Chien S *et al.* (2009) Stem cell fate dictated solely by altered nanotube dimension. *Proc. Natl. Acad. Sci. USA* **106**, 2130–2135.
16 Chamberlain LM, Brammer KS, Johnston GW, Chien S, Jin S (2011) Macrophage inflammatory response to TiO_2 nanotube surfaces. *J. Biomater. Nanobiotechnol.* **2**, 293–300.
17 Refai AK, Textor M, Brunette DM, Waterfield JD (2004) Effect of titanium surface topography on macrophage activation and secretion of proinflammatory cytokines and chemokines. *J. Biomed. Mater. Res. A* **70**, 194–205.
18 Roser K, Johansson CB, Donath K, Albrektsson T (2000) A new approach to demonstrate cellular activity in bone formation adjacent to implants. *J. Biomed. Mater. Res.* **51**, 280–291.
19 Lucas T, Waisman A, Ranjan R, Roes J, Krieg T, Muller W *et al.* (2010) Differential roles of macrophages in diverse phases of skin repair. *J. Immunol.* **184**, 3964–3977.
20 Park JY, Davies JE (2000) Red blood cell and platelet interactions with titanium implant surfaces. *Clin. Oral Implants Res.* **11**, 530–539.
21 Wozney JM (1998) The bone morphogenetic protein family: multifunctional cellular regulators in the embryo and adult. *Eur. J. Oral Sci.* **106**(Suppl 1), 160–166.
22 Wankell M, Munz B, Hubner G, Hans W, Wolf E, Goppelt A *et al.* (2001) Impaired wound healing in transgenic mice overexpressing the activin antagonist follistatin in the epidermis. *EMBO J.* **20**, 5361–5372.
23 Champagne CM, Takebe J, Offenbacher S, Cooper LF (2002) Macrophage cell lines produce osteoinductive signals that include bone morphogenetic protein-2. *Bone* **30**, 26–31.
24 Takebe J, Champagne CM, Offenbacher S, Ishibashi K, Cooper LF (2003) Titanium surface topography alters cell shape and modulates bone morphogenetic protein 2 expression in the J774A.1 macrophage cell line. *J. Biomed. Mater. Res. A* **64**, 207–216.
25 Chehroudi B, Ghrebi S, Murakami H, Waterfield JD, Owen G, Brunette DM (2010) Bone formation on rough, but not polished, subcutaneously implanted Ti surfaces is preceded by macrophage accumulation. *J. Biomed. Mater. Res. A* **93**, 724–737.
26 Yu WQ, Zhang YL, Jiang XQ, Zhang FQ (2010) In vitro behavior of MC3T3-E1 preosteoblast with different annealing temperature titania nanotubes. *Oral Dis.* **16**, 624–630.
27 Uttayarat P, Toworfe GK, Dietrich F, Lelkes PI, Composto RJ (2005) Topographic guidance of endothelial cells on silicone surfaces with micro- to nanogrooves: orientation of actin filaments and focal adhesions. *J. Biomed. Mater. Res. A* **75**, 668–680.
28 Jurukovski V, Dabovic B, Todorovic V, Chen Y, Rifkin DB (2005) Methods for measuring TGF-b using antibodies, cells, and mice. *Methods Mol. Med.* **117**, 161–175.
29 Chen S, Jones JA, Xu Y, Low HY, Anderson JM, Leong KW (2010) Characterization of topographical effects on macrophage behavior in a foreign body response model. *Biomaterials* **31**, 3479–3491.
30 Takebe J, Ito S, Champagne CM, Cooper LF, Ishibashi K (2007) Anodic oxidation and hydrothermal treatment of commercially pure titanium surfaces increases expression of bone morphogenetic protein-2 in the adherent macrophage cell line J774A.1. *J. Biomed. Mater. Res. A* **80A**, 711–718.
31 Yu W-Q, Qiu J, Zhang F-Q (2011) In vitro corrosion study of different TiO_2 nanotube layers on titanium in solution with serum proteins. *Colloids Surf. B* **84**, 400–405.
32 Khang D, Liu-Snyder P, Pareta R, Lu J, Webster TJ (2009) Reduced responses of macrophages on nanometer surface features of altered alumina crystalline phases. *Acta Biomater.* **5**, 1425–1432.
33 Zaveri TD, Dolgova NV, Chu BH, Lee J, Wong J, Lele TP *et al.* (2010) Contributions of surface topography and cytotoxicity to the macrophage response to zinc oxide nanorods. *Biomaterials* **31**, 2999–3007.
34 Waterfield JD, Ali TA, Nahid F, Kusano K, Brunette DM (2010) The effect of surface topography on early NFkappaB signaling in macrophages. *J. Biomed. Mater. Res. A* **95**, 837–847.
35 Kim JY, Khang D, Lee JE, Webster TJ (2009) Decreased macrophage density on carbon nanotube patterns on polycarbonate urethane. *J. Biomed. Mater. Res. A* **88**, 419–426.
36 Gongadze E, Kabaso D, Bauer S, Slivnik T, Schmuki P, van Rienen U *et al.* (2011) Adhesion of osteoblasts to a nanorough titanium implant surface. *Int. J. Nanomed.* **6**, 1801.
37 Gongadze E, Kabaso D, Bauer S, Park J, Schmuki P, Iglic A (2013) Adhesion of osteoblasts to a vertically aligned TiO_2 nanotube surface. *Mini Rev. Med. Chem.* **13**, 194–200.
38 Lavenus S, Ricquier JC, Louarn G, Layrolle P (2010) Cell interaction with nanopatterned surface of implants. *Nanomedicine (Lond.)* **5**, 937–947.
39 Davies JE (2003) Understanding peri-implant endosseous healing. *J. Dent. Educ.* **67**, 932–949.
40 Marchisio M, Di Carmine M, Pagone R, Piattelli A, Miscia S (2005) Implant surface roughness influences osteoclast proliferation and differentiation. *J. Biomed. Mater. Res. Part B* **75**, 251–256.
41 Kim YM, Kim MY, Kim HJ, Roh GS, Ko GH, Seo HG *et al.* (2011) Compound C independent of AMPK inhibits ICAM-1 and VCAM-1 expression in inflammatory stimulants-activated endothelial cells in vitro and in vivo. *Atherosclerosis* **219**, 57–64.